

Machine Learning to Characterize Hydro-Climate Impacts and Thresholds to Rainfed Agricultural Productivity

Ryan C. Johnson¹, Daniyal Hassan¹, Steven Burian¹, Carlos A. Oroza¹,
Marshall Shepherd², Vengus, Panhwar³

¹Civil and Environmental Engineering, University of Utah, Salt Lake City, UT, USA

²Department of Geography, University of Georgia, Athens, GA, USA

³Department of Civil Engineering, Mehran University of Engineering and Technology, Jamshoro, Sindh,
Pakistan

Key Points:

- Machine learning and remote sensing advance the understanding of rainfed agricultural system interactions.
- Phenology highlights constraining temperature- and precipitation-productivity feedbacks.
- Wheat yield is more sensitive to shooting phase sub-zero temperatures and low soil moisture.

Corresponding author: Ryan Johnson, ryan.c.johnson@utah.edu

Abstract

Sparse observational data in developing regions leads to uncertainty about how hydro-climatic factors influence crop phases and productivity, knowledge of which is essential to mitigating food security threats induced by climate change. In this study, NASA Tropical Rainfall Measuring Mission (TRMM), Global Precipitation Measurement (GPM), and Global Land Data Assimilation System (GLDAS) data products bypass spatiotemporal limitations and drive machine learning algorithms developed to characterize hydro-climate-productivity interactions. Extensive feature engineering processes these products into nearly 4000 metrics, designed to decompose crop growing season hydro-climate conditions. Dimensionality reduction with bidirectional step-wise regression, Multi-Adaptive-Regression-Splines (MARS), and Random Forest algorithms are explored to determine key temporal hydro-climate drivers to agricultural productivity, with each method recognizing unique linear and non-linear predictors. Finally, multi-variate regression, MARS, and Random Forest models are trained on the drivers to predict seasonal crop yield. We apply this hydro-climate-productivity framework to investigate *rabi* wheat productivity on Pakistan's Potohar Plateau. Here, we identify six of wheat's ten phenological phases that display strong hydro-climate responses, with the shooting phase exhibiting sensitivity to precipitation intensity, minimum soil moisture, and sub-zero temperatures. In addition, the plateau's heterogeneous climate-productivity connections are captured well by the calibrated models, strengthening their application for studying broader climate change impacts. The integration of remote sensing products and machine learning offers an effective framework to bypass in-situ data limitations and decompose climate-crop productivity relationships, thus improving drought onset recognition and food security forecasting.

1 Introduction

Rainfed agriculture produces over seventy percent of the world's staple crops to supply the majority of the food in developing nations (Kijne et al., 2003; Sharma et al., 2010). Rainfed (dryland) agriculture depends on unique hydro-climate (meteorological and environmental) growing season conditions for successful harvests—especially in satisfying soil moisture and water balance requirements (Hussain & Mudasser, 2007; Adnan et al., 2009; Kazmi & Rasul, 2009; Naheed & Mahmood, 2009; Sharma et al., 2010; Kazmi & Rasul, 2012; Gobbett et al., 2017). Favorable hydro-climate-productivity relationships are uncertain in a changing climate, especially in developing nations, where climate change has had and will continue to have disproportionate impacts (Hertel & Rosch, 2010). In these regions, crop tolerance limits are already challenged by existing soil moisture deficit, drought, high temperatures, high-intensity precipitation, and flood events (Parry, 2019). The International Panel of Climate Change (IPCC) anticipates additional climate non-stationary is very likely, which will accentuate existing plant moisture and thermal stresses (IPCC, 2006, 2014). Hence, characterizing non-stationary climate drivers to sustainably mitigate the consequences of climate change for food security is a high priority (Milly et al., 2008; Agovino et al., 2018; Karimi et al., 2018; Meijl et al., 2018; Mora et al., 2018).

In developing nations, sparse in-situ measurement networks and/or discontinuous time-series data compound the difficulty of characterizing hydro-climate-productivity responses (Jones et al., 2017). Surface water balance components, such as precipitation, temperature, and soil moisture, are difficult to obtain because of technical, monetary, and political limitations (Sheffield et al., 2006; Ghani et al., 2013). Where available, low-density observations (< 1 station per 20,000 km²) fail to capture complex land-surface hydrology interactions, including orographic precipitation (Worqlul et al., 2014; Mason et al., 2015). In the instances when long-term monitoring continuity is available, inadequate observational frequencies impair the investigation of these interactions (Alexander, 2016). Without an ample, continuous record of hydro-climate observations, crop yield forecasting is unlikely to improve.

Long-term, earth-monitoring, remote-sensing products may be able to circumvent limiting in-situ surface-atmosphere data. Lobell (2013) used remote sensing data to overcome both spatial and temporal scaling challenges in elucidating the crop yield gap in China, the United States, Mexico, India, and Brazil. In Pakistan, Ullah et al. (2019) found that gridded data products derived from remote sensing and re-analysis data show high correlations with in-situ daily precipitation measurements, making them suitable for hydrological studies. Since 2000, NASA's Tropical Rainfall Measurement Mission (TRMM), Global Precipitation Measurement (GPM), and Global Land Data Assimilation Systems (GLDAS) have been producing 3-hour continuous $0.25^\circ \times 0.25^\circ$ gridded observations (Adler et al., 2003; Rodell et al., 2004; Huffman et al., 2014). These datasets provide the necessary atmospheric and land surface data, in the form of surrogates for in-situ observations, to investigate agricultural hydro-climate-productivity responses in data-sparse regions (Collischonn et al., 2008; Awange et al., 2014).

Should adequate data be presented, extreme weather- and growing season-yield relationships offer preliminary frameworks for investigating hydro-climate-productivity interactions. Several single-factor analyses at phenological, monthly, and/or seasonal scales show noteworthy climate correlations and first-order constraining predictors (Rockström & Falkenmark, 2000; Kazmi & Rasul, 2009; Sun et al., 2010; Kazmi & Rasul, 2012). In Pakistan, Kazmi and Rasul (2012) identified a negative linear relationship between wheat yield and precipitation, and when separately evaluating minimum temperature influences, a positive relationship. Similarly, Zheng et al. (2018) found that for every one-day increase in a freezing event's duration, wheat grain yield decreased between 3.3-21.6% in parts of China. While these analyses characterize individual climate component relationships with crop survival, vigor, and final yield, these methods can offer only limited hydro-climate-productivity responses in coming decades, during which climatologists anticipate widespread hydro-climate non-stationarity as a result of climate change (IPCC, 2014; King et al., 2015; Mathew et al., 2018).

Numerous machine learning algorithms have improved yield forecasting performance. Kim et al. (2019) investigated several artificial intelligence (AI) methods in forecasting U.S. corn and soybean crops, finding that yields can be predicted accurately a month prior to harvest with an optimized deep neural network (DNN) model. In Brazil and the United States, Cunha et al. (2018) created a scalable machine learning system that took satellite-derived precipitation data, soil characteristics, and seasonal climate forecasts from physical models to deliver pre-season soybean and maize yield forecasts. Using Random Forests to predict wheat, maize, and potato yields, Jeong et al. (2016) found the algorithm to exceed multi-variate linear regression performance benchmarks when driven by global- and regional-scale climate and biophysical inputs. Although many ML algorithms show high yield forecasting performance, they can be limited in characterizing input-output variable interactions, are sensitive to noise, and do not generalize beyond the training data—a concern for climate change assessments. (Prasad et al., 2006; Bekhor & Livneh, 2012; Tang et al., 2018; Liakos et al., 2018; Kim et al., 2019; Cunha et al., 2018; Meng et al., 2017; Jeong et al., 2016; Ahamed et al., 2015).

Evaluating several yield-forecasting models driven by meteorological variables highlights the benefits and limitations of each method. Single-factor analysis is an important preliminary step in identifying relevant predictors via correlation coefficients and simple linear regression models. However, a single growing season variable lacks transmission of multi-variate interactions and feedbacks required to comprehensively describe and infer impacts to productivity. Advanced AI algorithms offer excellent predictive performance and low error. However, these methods are a “black box” regarding predictor-response interactions and often require high computational processing power (Prasad et al., 2006; Bekhor & Livneh, 2012; Tang et al., 2018; Liakos et al., 2018). Additionally, depending on the phenological phase, hydro-climate conditions share non-uniform relationships to photosynthetic rates, maturity, and yield (Hussain & Mudasser, 2007; Kazmi

& Rasul, 2009; Adnan et al., 2009; Sun et al., 2010; Kazmi & Rasul, 2012; Meng et al., 2017). Especially in data-sparse regions, relating unique hydro-climate conditions to phenological phase(s) improves yield feedback understanding.

Confronted by precipitation and temperature non-stationarity, improved characterization of rainfed agriculture productivity drivers will assist farmers and regional governments in improving food security and climate resilience. However, recent research has not decomposed hydro-climate impacts on rainfed agricultural productivity— primarily because of limited in-situ data. In responding to this gap in the research, we integrate NASA TRMM, GPM, and GLDAS data products into a multi-model approach that circumnavigates pre-existing data and methodological limitations. Hence, our framework benefits from stepwise regression (SWR), multi-variate linear regression (MLR), multi-adaptive-regression-splines (MARS), and Random Forest regression (RFR) algorithms to identify crop phenological importance (i), driver-yield impacts (ii), and crop productivity-thresholds (iii). To investigate the framework’s real-world application, we apply these methods to Pakistan’s Potohar plateau as a pilot study. Operating under the hypothesis that phenology-aligned climate conditions drive crop productivity, we determine key *rabi* wheat hydro-climate drivers and their respective impacts on seasonal yield. With the pilot study success, this framework demonstrates potential for implementing data-backed policies, decision-making, and infrastructure planning, ultimately supporting the effort to improve seasonal yield forecasts, mitigate long-term climate-yield impacts, and enhance food security.

2 Methodology

2.1 Feature Engineering

We overcome in-situ data constraints by using Google Earth Engine (GEE) to access the increased spatiotemporal resolution and data continuity of NASA TRMM, GPM, and GLDAS data products. TRMM and GPM provide precipitation data and GLDAS provides air temperature, soil temperature, and soil moisture data from 2000 to present. We employ extensive feature engineering to align hydro-climate conditions with plant phenology. This begins by aggregating the 3-hour temporal resolution data into weekly, monthly, and growing season periods (n). For each period minimum, mean, and maximum statistical metrics are developed for air temperature, soil moisture, and soil temperature and cumulative (mm) for precipitation. Table 1 displays these statistical metrics.

Table 1. Weekly, monthly, and growing season air temperature (A_T), precipitation (P), soil temperature (S_T), and soil moisture (S_M) statistical metrics are matched to crop phenology.

Metric	Statistic	Description
Precipitation		
$P(n)$	$\sum^n P$	Cumulative P (mm)
Air / Soil Temperature		$^{\circ}C$
$A_T(n), S_T(n)$	$A_T, S_T(min_n, mean_n, max_n)$	min, mean, and max A_T, S_T
Soil Moisture		kg/m^2
$S_M(n)$	$S_M(min_n, mean_n, max_n)$	min, mean, and max S_M

Table 2. The higher temporal resolution NASA data products permit metrics capturing unique weekly, monthly, and growing season soil temperature (S_T), air temperature (A_T), and precipitation (P) conditions.

Metric	Statistic	Description
Soil/Air Temperature		
$A_{Thrs}(n), S_{Thrs}(n)$	$\sum^n A_T, S_T < 0$	*Hrs with $A_T, S_T < 0^\circ C$
$A_{Thrs}(n), S_{Thrs}(n)$	$\sum^n 0 < A_T, S_T < 10$	*Hrs with $A_T, S_T: 0 - 10^\circ C$
$A_{Thrs}(n), S_{Thrs}(n)$	$\sum^n 10 < A_T, S_T < 20$	*Hrs with $A_T, S_T: 10 - 20^\circ C$
$A_{Thrs}(n), S_{Thrs}(n)$	$\sum^n 5 < A_T, S_T < 15$	*Hrs with $A_T, S_T: 5 - 15^\circ C$
$A_{Thrs}(n), S_{Thrs}(n)$	$\sum^n 15 < A_T, S_T < 25$	*Hrs with $A_T, S_T: 15 - 25^\circ C$
$A_{Thrs}(n), S_{Thrs}(n)$	$\sum^n A_T, S_T > 20$	*Hrs with $A_T, S_T > 20^\circ C$
Precipitation		
$P_{Ihrs}(n)$	$\sum^n 1 < P_I < 5$	*Hrs with $P_I: 1-5$ mm/hr
$P_{Ihrs}(n)$	$\sum^n 5 < P_I < 8$	*Hrs with $P_I: 5-8$ mm/hr
$P_{Ihrs}(n)$	$\sum^n 8 < P_I < 15$	*Hrs with $P_I: 8-15$ mm/hr
$P_{Ihrs}(n)$	$\sum^n P_I > 15$	*Hrs with $P_I > 15$ mm/hr
$P_{Ihrs}(n)$	$\sum^n P_I < 8$	*Hrs with $P_I < 8$ mm/hr
$P_{Ihrs}(n)$	$\sum^n P_I > 8$	*Hrs with $P_I > 8$ mm/hr
$P_{Imax}(n)$	$\max_n(P_I)$	P_I Max mm/hr
$P_d(n)$	$\sum^n P_{day} > 3$	**Days with $P > 3mm$
$P_{\overline{F}}(n)$	$\sum^n \frac{P_d}{n_{days}}$	***Precipitation Frequency
$P_{d_{mw/o}}(n)$	$\max_n \sum^n P_d = 0$	**Max Consecutive $P_d = 0$
$P_{d_{w/o}}(n)$	$\text{mean}_n \sum^n P_d = 0$	**mean Consecutive $P_d = 0$

A second set of metrics emphasizes air and soil temperature characteristics, specifically the number of hours above, below, or between specified thresholds, see Table 2. As an example, equation 1 is used to aggregate the quantity of observations (A_T) in hours during which temperatures were below the threshold ($X^\circ C$) to produce an air temperature threshold-hour (A_{Thrs}) metric. This framework is applied to develop additional A_{Thrs} metrics counting the quantity of hours between and greater than a range of $X^\circ C$ values. As a result, the metrics, in hours per temporal period (n), aid in identifying a range of damaging and constructive productivity temperatures with respect to crop phenology.

$$A_{Thrs}(n) = \sum_0^n A_T < X^\circ C \quad (1)$$

This second set of metrics is also applied to precipitation because of the focus on rainfed agriculture. Since plant water requirements are satisfied via precipitation, we developed a variety of metrics emphasizing precipitation intensity and drought (precipitation frequency) at weekly, monthly, and seasonal temporal scales. Precipitation intensity (P_I) metrics consist of the quantity of hours ($P_{Ihrs}(n)$, *hrs*) below, between, or above predetermined thresholds and also includes the maximum intensity ($\max_n(P_I)$, *mm/hr*) per period. The purpose of these metrics is to distinguish precipitation events that cause overland flow, and possibly crop destruction, from those that do not generate runoff.

The drought metrics decompose each period's precipitation regime, consisting of per-period precipitation days ($P_d(n)$), precipitation frequency ($P_F(n)$), maximum consecutive days without precipitation ($P_{Mw/o}(n)$), and mean days without precipitation ($P_{w/o}(n)$). Precipitation days counts the number of days per period of greater than 3mm of rain per 12 hours, the standard for measurable rainfall (NOAA, 2020). Precipitation frequency is similar to precipitation days but normalized as a ratio of days with measurable rainfall divided by the total number of days in the period (*days/period*). This metric describes how frequently precipitation occurs in a given period. Maximum consecutive days without precipitation identifies prolonged periods with no measurable precipitation, which are known to strongly influence crop yield (Rockström & Falkenmark, 2000). Lastly, mean consecutive days without precipitation ($P_{w/o}(n)$, *days*) further describes growing season drought conditions by recognizing the average consecutive number of days per period not receiving measurable precipitation. Table 2 outlines the comprehensive set of air temperature, soil temperature, and precipitation metrics. Altogether, nearly 4000 weekly, monthly, sub-season, and seasonal hydro-climate predictors are created for a typical six-month seasonal crop lifecycle.

2.2 Dimensionality Reduction and Driver Selection

The feature engineering process leads to high data-dimensionality, offering little guidance to characterize hydro-climate-productivity relationships. We respond to the high dimensionality by integrating statistical measures and machine learning to systematically reduce the number of variables and identify the most influential hydro-climate drivers. Throughout this process, we apply the parsimony principle to manage complexity, overfitting, and collinearity. Our variable reduction framework first begins by segregating air temperature, precipitation, soil moisture, and soil temperature variables. Then, for each category, each metric's correlation with crop productivity is determined and those with a Pearson's correlation coefficient (ρ) greater than 0.40 are kept to produce four correlated feature sets (CFS). Metrics with ρ less than 0.40 are interpreted as poor productivity indicators and are removed from the study. Each CFS is then used to drive several machine learning algorithms that select linear (SWR), threshold (MARS), and non-linear (RFR) hydro-climate drivers with crop productivity. Lastly, the selected CFS predictors are aggregated into a hydro-climate variable set where the algorithms are re-applied to deliver three final sets of hydro-climate drivers, one set for each algorithm. The machine learning processes are further described in the subsequent sections, with the workflow illustrated in Figure 1.

Stepwise Regression

Stepwise regression selects features as a function of their statistical significance to the response variable, which is, in this case, crop productivity. Both Hocking (1976) and Draper (1981) describe the fundamental basis and details of the stepwise (forward, backward, bidirectional) variable selection processes. In RStudio, bidirectional SWR trained on a randomly selected 75% data subset, five-fold cross-validation, and a minimized root-mean-squared-error (*RMSE*) determine categorical predictors, significantly (*p-value* <

0.05) contributing to yield. Within each category, a colinearity test is performed, equation 2, where ρ is calculated between two selected features.

$$Colinearity = \frac{1}{1 - \rho^2} \quad (2)$$

If the co-linearity test exceeds 10, the process removes the less significant predictor and re-evaluates the model. Upon completion of SWR variable selection, a final model run and colinearity test with all categorical features identifies the statistically significant hydro-climate drivers.

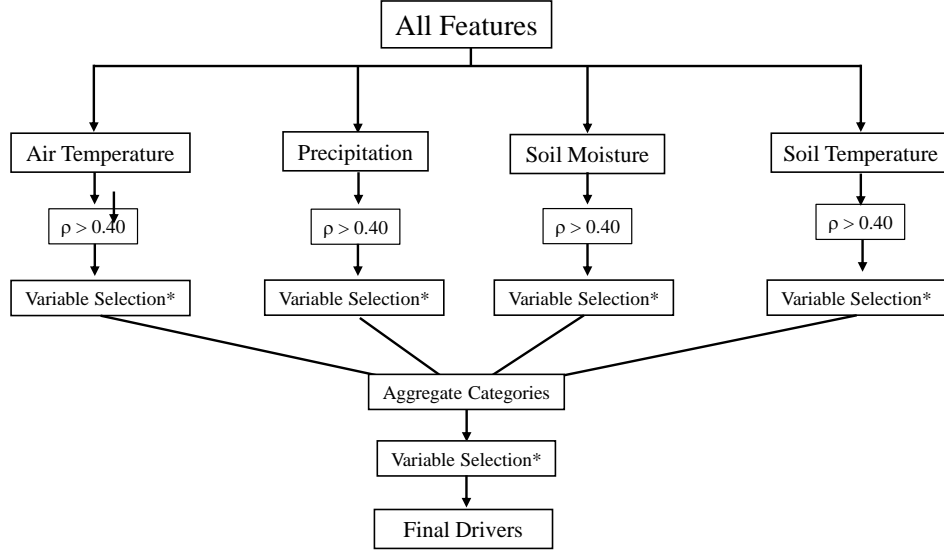


Figure 1. Nearly 4000 possible hydro-climate variables are separated into their respective categories (A_T , S_T , S_M , & P). *Includes SWR, RFR, and MARS feature selection techniques.

Random Forest

Our second feature reduction technique utilizes Random Forests, a non-parametric algorithm based on decision trees. It operates as a meta-estimator, fitting several regression-based decision trees on multiple subsamples of the datasets, and then averages all the trees to improve predictive accuracy and robustness (Breiman, 2001; Biau & Scornet, 2016; Geurts et al., 2006). Random Forest's feature importance is a prominent algorithmic element of this study, enabling limited internal modeling transparency in order to discern algorithm function and generate coherent predictor-yield evaluations. This output scales the relative importance of each input feature's reduction in variance across the forest (Pedregosa et al., 2011; Buitinck et al., 2013; Boschetti & Massaron, 2018). As a result, the input variables used more often in decision making produce larger values and indicate greater importance in predicting crop yield.

We employ SciKitLearn 0.24.0 RandomForestRegressor as the Random Forest algorithm, trained on the same randomly selected 75% data subset as SWR (Pedregosa et al., 2011). The algorithm is optimized using a five-fold cross-validation and GridSearchCV function to determine the hyperparameters by a "fit" and "score" method to minimize *mean-squared-error (MSE)*. Within this function, we used a wide search grid to ensure correct algorithm calibration: number of estimators from 400-4000 at 200-unit intervals, max depth between 5-65 at 5-unit intervals, and max predictors 0.25 - 1.0 at 0.25-unit intervals. The algorithm's calibrated hyper-parameters should not fall on the limits of the search grid.

In Random Forest, an iterative approach considering feature importance, model performance, and colinearity forms the predictor reduction process. Beginning with the CFS, Random Forest iteratively selects the top-50% most important features. At each iteration, model predictive performance ($RMSE$, MSE , MAE) is assessed to ensure it did not decline as a result of fewer feature inputs. Due to Random Forest's ability to cope with co-linearity, several features produced colinearity scores greater than 10. In this situation, model runs were repeated after removal of co-linear features of lesser importance, until the top-five features passed the colinearity test. The final steps aggregate all categorical feature sets, iteratively reduce the sets by the least important predictor until model performance decreases, and apply a final colinearity test.

Multi Adaptive Regression Splines

We employ RStudio's Earth package as our MARS algorithm. The algorithm performs automated variable reduction, adding and removing features in a pruning process. Like RFR, MARS includes a feature importance measure, reflecting the RSS error associated with feature addition or removal (UCR, 2018). This process evaluates the residual sum of squares (RSS) as a new variable is added or subtracted, obviating the need for manual iterations to reduce variables. Features that strongly assist RSS reductions have greater importance to the model and are kept, whereas features that do not strongly influence RSS reductions are removed. Within the modeling process, a hyper-parameter grid search across predictor interaction degrees (1, 2, 3) and predictor pruning (2-20, by a unit of 1) is conducted over a five-fold cross-validation, with the model tuned to minimizing $RMSE$. The calibrated MARS algorithm quickly reduced predictors in each CFS and the final aggregated CFS, delivering features with little colinearity.

2.3 Determining Phenological Importance, Impact, and Thresholds

We identify and characterize hydro-climate drivers and their respective phenological importance, impact, and thresholds to productivity in data-poor regions. Phenological importance is defined as the temporal period in which a driver occurs (ex. Week 15, and using Table 4, shooting phase), with additional importance criteria supplied by the observation category and metric (ex. air temperature: minimum). Using this classification approach, our qualitative phenological importance assessment aggregates the number of hydro-climate drivers per phase, operating under the assumption that more hydro-climate sensitive phases contain more drivers. The added category and metric criteria clarifies which hydro-climate components display importance at specific crop phases. We also perform a quantitative phenological importance assessment using the calibrated Random Forest feature importance. Here, we compare each driver's importance as well as aggregate driver importance by phase to provide an indicator of which growth stages are the most hydro-climate sensitive with regard to crop productivity.

The hydro-climate impact assessment characterizes each driver's linear relationship to crop productivity. We use RStudio to develop three MLR models for each set of drivers, calibrated with a five-fold cross-validation scheme and tuned via MSE Equation 3 to display the general form of the algorithm.

$$Yield = \alpha + \beta_1 x_1 + \beta_2 x_2 + \dots + \beta_n x_n \quad (3)$$

The slope, β , represents the impact per driver's unit increase with positive or negative relationships depending on coefficient sign.

We further investigate hydro-climate-productivity impacts through a normalized comparison of minimum, mean, and maximum driver set interactions. In this framework, these driver observations are retrieved from the NASA data products period of record

(2000 to 2017) and placed into Equation 4, where d refers to a driver of interest within a driver set (from SWR, MARS, or RFR).

$$dNI_{min,mean,max} = \frac{\beta_d x_d}{Yield} * 100\% \quad (4)$$

In determining each driver's normalized minimum impacts, all minimum drivers are independently multiplied by their respective β from the calibrated MLR models (Equation 3) and then divided by the predicted yield using the driver set's minimum observations. This ratio is then multiplied by 100% to reveal each minimum driver's percentage-wise contribution to yield. Calculation of normalized mean and maximum impacts are performed in a duplicate fashion. By classifying and calculating normalized impact in this manner, the hydro-climate drivers imposing limiting and supporting conditions to crop productivity are highlighted.

Thresholds are key values which, when met or exceeded, result in a measurable driver-response change. The MARS algorithm's non-parametric approach identifies a driver's threshold via hinge functions and their piece-wise linear relationship with productivity, see equation 5 (Friedman, 1991). Here, h represents the slope coefficient, d represents the driver of interest, and α represents the threshold.

$$h(d - \alpha) \quad (5)$$

The hinge function only activates when $(d - \alpha)$ or $(\alpha - d)$ is positive— otherwise the equation's value is zero.

2.4 Pilot Study Description

Pakistan is a top-10 international wheat exporter with approximately 26% of its cultivated area devoted to rainfed agriculture (Kazmi & Rasul, 2012). The Potohar plateau, in the country's northeastern quadrant, as illustrated in Figure 2, is one of its most productive and researched rainfed regions. The region's location, surrounded by mountainous terrain and large rivers, creates advantageous soil and climate conditions for winter (*rabi*) and summer (*kharif*) rainfed crops. At a finer spatial resolution, the plateau's hilly topography and steep hill slopes present many challenges to reliable crop yields. First, the steep slopes allow for high precipitation intensities to cause erosion and remove fertile top soil. Second, while surrounded by rivers, the topography has prevented the region's connection to the Indus Basin Irrigation System (IBIS) and, therefore, is much more likely to be negatively impacted by droughts than adjacent irrigated areas (Baig et al., 2013).

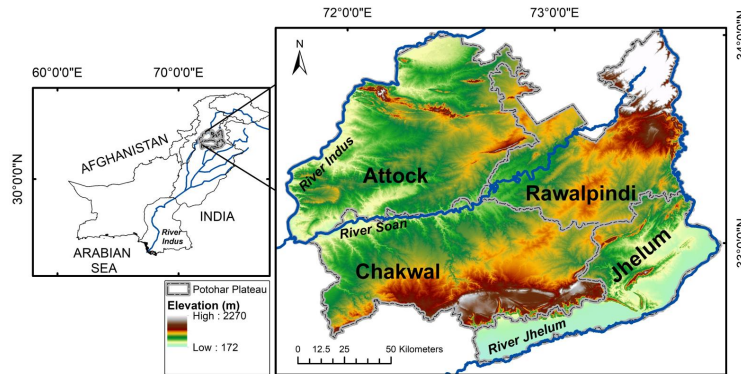


Figure 2. The surrounding mountainous terrain challenges climate data extrapolation but, in conjunction with large river systems, creates an excellent environment for rainfed agriculture

The Potohar plateau shares similarities with other developing nations' meteorological networks, as station density is approximately one per twenty-thousand km^2 (Mason et al., 2015). Although they support rainfed agriculture, the topographic features compromise spatial extrapolation of in-situ meteorological data. These data limitations impact not only hydro-climate-productivity research, but also hydrological condition assessments, drought monitoring, and other hydro-climate applications (Adnan et al., 2009; Kazmi & Rasul, 2009, 2012; Mason et al., 2015). Thus, given the combination of the region's dependence on *rabi* wheat as a food source, the coarse and discontinuous meteorological observations, and future climate uncertainty, the location is as an excellent pilot study area to apply the NASA data product-machine learning framework to investigate hydro-climate-productivity relationships.

Table 3. The four districts show heterogeneity in growing season precipitation, air temperature, and resulting yield

Metric	Attock	Chakwal	Jhelum	Rawalpindi
Minimum Precipitation (mm)	15.9	9.9	12.4	17.8
Mean Precipitation (mm)	79.1	64.0	63.5	86.9
Median Precipitation (mm)	55.5	47.6	51.8	70.1
Maximum Precipitation (mm)	181.7	162.1	158.9	220.6
Mean Minimum Temperature ($^{\circ}C$)	1.7	2.4	3.6	2.1
Mean Temperature ($^{\circ}C$)	13.6	13.5	14.8	13.2
Mean Maximum Temperature ($^{\circ}C$)	29.6	29.3	30.8	29.2
Minimum Yield (tones/ha)	0.7	0.6	0.8	0.6
Mean Yield (tones/ha)	1.4	1.3	1.7	1.5
Median Yield (tones/ha)	1.5	1.2	1.7	1.6
Maximum Yield (tones/ha)	2.0	1.8	2.2	2.0

For each district in Potohar, NASA TRMM, GPM, and GLDAS data products from 2000 to 2017 were collected and averaged to a district spatial resolution. This aligns with Punjab's Department of Statistics (2018) reported total wheat yield (tones) and tilled area (hectares). Although the study period extends over eighteen years, heavy monsoons in 2009 caused devastating flooding and erosion, leading many farmers to not sow *rabi* crops. Thus, this year was omitted from the analysis. Using the NASA data products and preliminary data processing, Table 3 displays *rabi* growing season precipitation and temperature statistics in each district. For comparison, the table also includes wheat productivity statistics over the equivalent study period.

Table 4. Potohar wheat phenology with Week ID expressing the number of weeks post-seeding.

Phase #	Phase	Period	Week ID
1	Emergence	Nov 15 - 30	3-4
2	Third Leaf	Dec 01 - 20	5-7
3	Tilling	Dec 21 - Jan 15	8-10
4	Shooting	Jan 16 - Feb 25	11-15
5	Heading	Feb 26 - Mar 05	16
6	Flowering	Mar 06 - 20	17-18
7	Milk Maturity	Mar 21 - Apr 18	19-22
8	Wax Maturity	Apr 19 -25	23
9	Full Maturing	Apr 26 - 28	24
10	Harvest	Apr 29+	25+

Analysis of the Potohar plateau hydro-climate data and wheat yield display heterogeneity among districts. Evaluating hydro-climate, *rabi* growing season conditions mostly differ in precipitation, as mean and maximum air temperatures display less variability and differences among districts. District-wise, Jhelum consistently experiences warmer minimum, mean, and maximum temperatures and Rawalpindi receives the greatest winter precipitation. Similar to hydro-climate conditions, wheat yield varies across years and districts. As sowing dates are consistent among districts and years, we hypothesize that each district's unique growing season climate conditions lead to differences wheat productivity. Among the Potohar plateau districts, Jhelum consistently delivers the greatest wheat yields, while Chakwal routinely produces the lowest.

Potohar's wheat phenology forms the foundation for each temporal period's significance for productivity, beginning with seed sowing in late October/early November and harvest completion in late April/early May (Kazmi & Rasul, 2012). Aligning hydro-climate conditions with Table 4's phenological phases establishes a position to investigate meteorological and environmental influences at specific growth stage(s) and resulting grain harvest impacts.

Table 5. Feature engineered NASA data products and machine learning variable selection techniques identify twenty-one unique hydro-climate drivers.

Driver	Model	Phase	Impact
WK 10 $A_T \max$	MARS	Tillering	+
Jan $S_{M\max}$	RFR	Tillering, Shooting	+
WK 11 $A_T \min$	MARS	Shooting	+
WK 13 $S_M \max$	RFR	Shooting	+
WK 14 $A_T \min$	MARS, SW	Shooting	+
WK 14 $S_M \min$	RFR	Shooting	-
WK 14 $S_{Thrs} > 10^\circ\text{C}$	RFR	Shooting	+
WK 15 $A_T \min$	MARS	Shooting	-
WK 15 $S_T \min$	RFR	Shooting	+
WK 15 $S_M \text{ mean}$	SW	Shooting	+
Feb $S_M \min$	RFR	Shooting	+
Feb $S_M \text{ mean}$	MARS	Shooting	+
WK 16 $S_{Thrs} > 10^\circ\text{C}$	RFR	Heading	+
WK 16 $S_M \min$	RFR	Heading	-
Jan & Mar $P_{Ihrs} < 8$	SW	Tillering, Shooting,	+
$\frac{\text{mm}}{\text{hr}}$		Flowering, Milk Maturity	
WK 23 $A_T \max$	MARS	Wax Maturity	+
WK 23 $S_T \min$	MARS	Wax Maturity	-
WK 24 $S_{Thrs} > 10^\circ\text{C}$	RFR	Wax Maturity	+
Max Monthly P	MARS, RFR	Shooting, Heading,	-
		Flowering	
Season P	RFR	Shooting, Heading,	+
		Flowering	
Season $S_T \min$	SW	Third Leaf, Tillering	+

In order to evaluate the application of the NASA data-machine learning methods, all Potohar districts' hydro-climate and wheat productivity data are aggregated into a single regional data frame, operating under the assumption that hydro-climate conditions share similar productivity influences throughout the plateau. This results in sixty-four seasonal wheat harvest observations for variable selection and algorithm calibration/validation.

The variable selection processes proceeded smoothly with minimal user input. The correlated feature sets reduced the ~ 4000 initial features down to ~ 550 . Using SWR, RFR, and MARS algorithms, post co-linearity reduction yielded four, eleven, and eight hydro-climate drivers, respectively, per variable reduction method. The RFR variable reduction method produced co-linear predictors, requiring modeler interactions at each iteration. Here, small model performance improvements were observed at each iteration. The RFR algorithm also required significantly longer calibration time, a result of the extensive hyper-parameter search. All together, these methods collectively identified twenty-one unique hydro-climate drivers. Table 5 displays each algorithm's drivers with their temporally aligned phenological phase and MLR coefficient sign with productivity.

3 Results

High algorithm predictive performance is necessary to characterize hydro-climate phenological importance, impact, and thresholds. First, for each algorithm (MLR, MARS, and RFR) and driver set (SWR, MARS, and RFR) combination we evaluate modeling performance using a validation dataset comprised of the remaining 25% unseen hydro-climate and productivity data (Section 3.1). This section provides the foundation to quantitatively assess hydro-climate-productivity relationships and limitations. Section 3.2 discusses the connections among hydro-climate drivers and wheat phenology. Section 3.3 characterizes each driver's impact to wheat productivity and Section 3.4 examines driver-productivity thresholds.

3.1 Model Performance

Nearly all driver-algorithm pairings produced satisfactory model performance to investigate hydro-climate-productivity cause-effect relationships. Table 6 displays each driver set and algorithm's "goodness of fit" measures. Subsequently, we also conducted a residual analysis to determine each pairing's modeling proficiency for low, medium, and high yields. This analysis benchmarks an algorithm's ability to characterize drivers and determines limiting and supportive relationships, thus validating our methodology and promoting in-depth hydro-climate-productivity relationship evaluation. Validating model proficiency across the spectrum of low to high yield is also critical to facilitate improved crop forecasting and climate change impacts, especially in the context of anticipated aridity increases, warmer temperatures, and altered precipitation regimes.

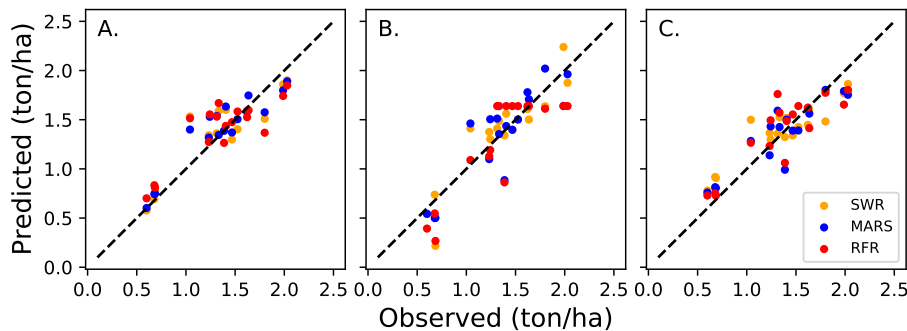


Figure 3. SWR and MARS drivers display high model performance within the MLR (A), MARS (B), and Random Forest (C) algorithm. Random Forest drivers displayed the highest deviations from the validation dataset in the MARS (B) algorithm.

The MLR algorithm displays high model performance for all driver pairings, especially with SWR and MARS drivers, indicating strong linear interactions. Decompos-

ing MLR-SWR drivers, correct low yield predictions suggest the correct capture of productivity-limiting hydro-climate influences. In response to the SWR variable selection process, all drivers are statistically significant with a p -value < 0.05 . The MARS driver set's added dimensionality, eight vs four, likely holds responsibility for low to medium yield prediction's residual reduction, resulting the study's highest modeling performance. The Random Forest driver set displayed increased low and high yield residual errors in comparison to the SWR and MARS driver sets. This is likely the result of Random Forest's non-parametric architecture, which selected drivers not limited by linear relationships with crop productivity. Further, the MLR algorithm failed to model these non-linear relationships, and, per the residual analysis, we dismiss the Random Forest driver set from the impact portion of the study. The validated MLR algorithm pairing with SWR and MARS drivers provides the analytical foundation for the impact study.

Table 6. Nearly all driver-algorithms pairings display high model performance.

Predictor Set	Model	MAPE (%)	RMSE	R ²
MARS	MLR	9.7	0.16	0.85
RFR	MLR	14.3	0.22	0.77
SWR	MLR	9.9	0.18	0.82
MARS	MARS	14.3	0.22	0.77
RFR	MARS	17.7	0.26	0.73
SWR	MARS	12.9	0.19	0.84
MARS	RF	12.7	0.18	0.81
RFR	RF	12.9	0.21	0.75
SWR	RF	14.9	0.20	0.83

The MARS algorithm displayed ample modeling performance for SWR and MARS drivers. Here, SWR drivers showed a slight improvement over MARS drivers in predicting wheat yield between 1.1-1.7 tones/ha. Additionally, only *Week 15 Mean Soil Moisture* displayed a threshold and is further discussed in Section 3.4. When comparing SWR and MARS driver sets' low- and high-yield predictions with those from the MLR algorithm, we observed slightly increased residuals. The Random Forest drivers and MARS algorithm produced the study's poorest model performance. This was the result of thresholds modeling observed yields of 1.25 tones/ha and greater as 1.6 tones/ha, significantly suppressing predictive performance. As concluded in the impact analysis, Random Forest drivers are determined to be unfit for the investigation of hydro-climate thresholds. The validated MARS algorithm pairing with SWR and MARS drivers provides the analytical foundation for the hydro-climate threshold portion of the study.

Random Forest's algorithm architecture delivers acceptable predictive performance across all driver sets. While still lower than SWR and MARS driver sets, Random Forest drivers produced their highest model performance compared to MLR and MARS algorithms. For all driver sets, the algorithm captures low yields and demonstrates sufficient modeling performance to permit feature importance evaluation.

3.2 Phenological Importance

Two methods evaluate hydro-climate and phenological importance by: 1) matching each driver's temporal period with wheat's phenological phase(s) and 2) using Random Forest feature importance. Evaluating hydro-climate temporal properties in Table 5 and 7, all phases but full maturity and harvest are present. Aggregating all drivers per phase shows that 45% occur during shooting, 13% in heading, 13% in tillering, 13% in

wax maturity, 10% in flowering, 3% during third leaf, and 3% during milk maturity. These values take into account cases in which a driver's temporal boundaries extend across multiple phases. Table 5 displays the drivers and their respective phase(s). No drivers per phase exhibit strong colinearity, validating each driver's unique phenological contribution.

Hydrological drivers, precipitation and soil moisture, are more numerous and display greater feature importance than temperature-based drivers. Summing hydrologic drivers reveals they form 62% of the total drivers vs. 38% related to temperature. Precipitation's strong influence on productivity is further emphasized by the fact that it holds the greatest feature importance in MARS and RFR driver sets, nearly a 2-fold increase over the next driver's importance, see Figure 4. While expected, the algorithm's ability to recognize hydrological driver importance in a precipitation-dependent agrarian system further validates the modeling framework. Additionally, Random Forest's feature importance characterization provides a quantitative mechanism to connect hydro-climate limiting, and reinforcing, conditions with Potohar's wheat productivity.

Table 7. The quantity of drivers per category and phase are shown in the matrix. By aggregating all precipitation and soil moisture drivers, their majority percentage leads to the conclusion that hydrological drivers are the most influential to wheat productivity.

Phase	A_{min}	A_{max}	P	S_{Moist}	S_{Tmin}	$S_{T>10^{\circ}C}$	Σ	%
Third Leaf	-	-	-	-	1	-	1	3
Tillering	-	1	1	1	1	-	4	13
Shooting	3	-	3	6	1	1	14	45
Heading	-	-	2	1	-	1	4	13
Flowering	-	-	3	-	-	-	3	10
Milk Maturity	-	-	1	-	-	-	1	3
Wax Maturity	-	1	-	1	1	1	4	13
Σ	3	2	10	9	4	3	31	-
%	10	6	32	29	13	10	-	100

Aggregating SWR, MARS, and RFR hydro-climate driver feature importance per phenological phase from Figure 4 displays the shooting phase accounting for 80%, 79%, and 75%, respectively. Note that phase-specific feature importance aggregates individual driver importance such that aggregated phase importance can exceed 100%. This indicates that wheat's shooting phase is strongly influenced by hydro-climate conditions and is a critical phenological stage to a successful wheat harvest. During this phase, minimum air temperatures, precipitation quantity, soil moisture levels, and minimum soil temperatures, and hours above 10°C yield the greatest feature importance. The ordering of the remaining phases based on Random Forest feature importance is inconsistent, which hinders further analysis in this pilot study.

Recognizing these key drivers' phenological timing and importance provides farmers and agricultural agencies with key information to maintain and improve crop productivity; more in Section 4.2.

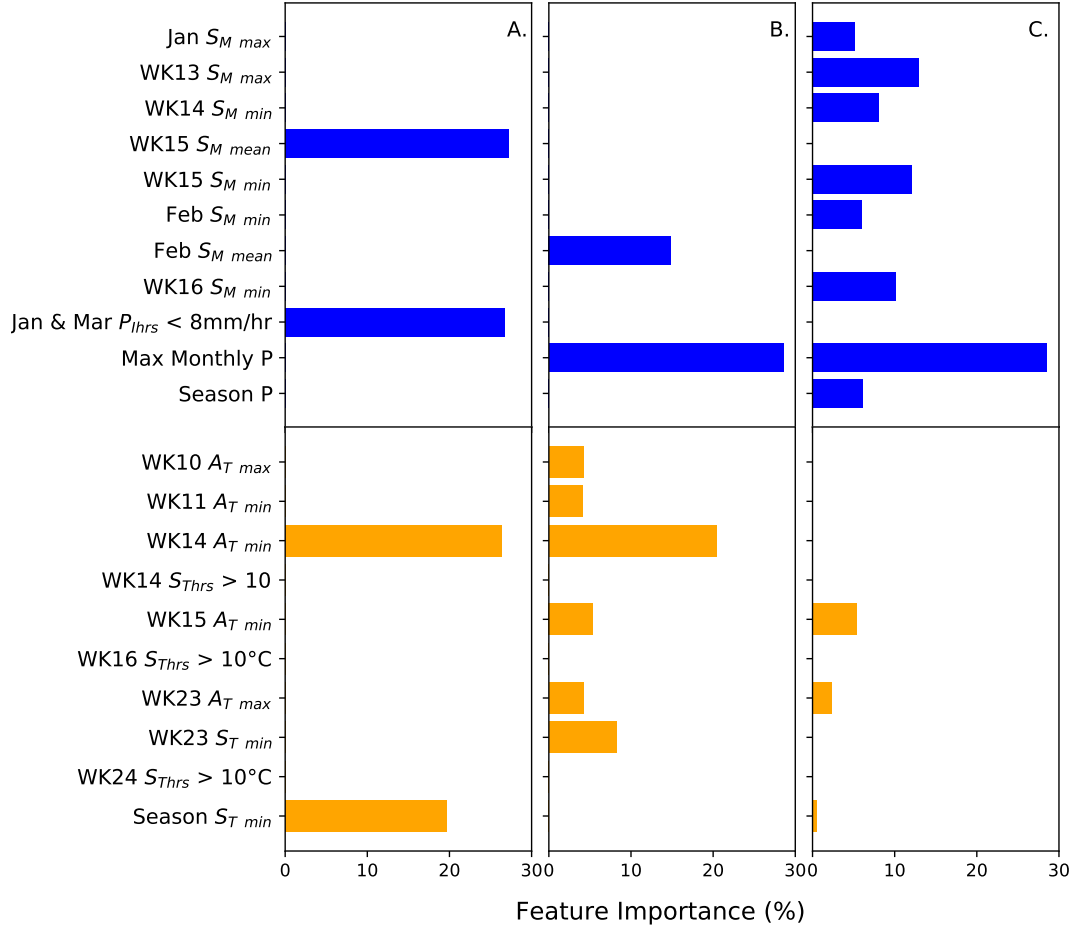


Figure 4. Random Forest identifies hydrological (blue) drivers in the shooting, heading, and flowering phases displaying high feature importance within SWR (A), MARS (B), and Random Forest (C) drivers sets. The algorithm also highlights air and soil temperatures (orange) during the shooting phase with high importance.

3.3 Impact

The MLR algorithm identifies key statistical relationships between phenological hydro-climate conditions and productivity. Among SWR drivers, *week 15 soil moisture* contributes the most to productivity (33%-133%) at a rate of 0.03 tones/ kg/m^2 , Table 8. This predictor is dominant during episodes of low air/soil temperature and low precipitation. Precipitation positively influences yield, with each additional hour of *January & March precipitation intensity hours $\leq 8 \text{ mm/hr}$* contributing 0.01 tones. While no outstanding co-linearity exists between *week 15 soil moisture* and *January & March precipitation intensity hours*, increased duration of low-intensity precipitation is sure to reinforce supportive soil moisture conditions during the most critical phenological phase (shooting).

Evaluating wheat productivity responses to SWR air and soil temperature drivers indicates that above-freezing minimum temperatures are beneficial. This is relayed via positive driver coefficients, see Table 8. Again, coinciding with the shooting phase, low *Week 14 minimum air temperatures* do not support favorable growing conditions and sub-zero temperatures induce a negative response. This relationship is also present for *season minimum soil temperature* with a rate -0.12 tones per degree sub-zero.

Table 8. Among both SWR and MARS drivers, soil moisture is a leading hydro-climate component that positively impacts productivity.

Driver	Coef Val	Min Obs	Mean Obs	Max Obs	Min Cont	Mean Cont	Max Cont	Min %	Mean %	Max %
SWR										
Intercept	0.17	-	-	-	-	-	-	-	-	-
WK 14 A_{min}	0.06	-0.6	5.8	10.8	-0.03	0.33	0.61	-12	25	26
WK 15 $S_{mean\ Moist}$	0.03	14.0	23.0	32.6	0.35	0.57	0.82	133	44	34
Jan & March $P_{it} < 8\text{ mm/hr}$	0.01	0.00	29.3	75.0	0.00	0.19	0.48	0	14	20
Season $S_{min\ Temp}$	0.12	-0.5	2.0	4.4	-0.05	0.21	0.46	-21	16	20
MARS										
Intercept	-0.38	-	-	-	-	-	-	-	-	-
WK 10 A_{max}	0.03	15.5	20.1	24.9	0.53	0.69	0.85	104	53	50
WK 11 A_{min}	0.07	-3.2	4.7	9.9	-0.21	0.31	0.65	-41	24	39
WK 14 A_{min}	0.09	-0.6	5.8	10.8	-0.05	0.55	1.02	-11	42	60
WK 15 A_{min}	-0.06	1.6	6.4	12.0	-0.10	-0.38	-0.72	-19	-29	-42
Feb $S_{mean\ Moist}$	0.03	13.4	23.3	30.9	0.44	0.77	1.02	87	59	60
WK 23 A_{max}	0.03	28.7	34.3	41.5	0.87	1.05	1.26	171	80	74
WK 23 $S_{min\ Temp}$	-0.08	11.7	21.2	30.0	-0.97	-1.65	-2.34	-192	-126	-138
Max Monthly P	-0.001	4.9	36.4	82.2	0.00	-0.02	-0.05	-1	-2	-3

The eight MARS drivers reveal both positive and negative coefficients that support and compromise productivity, Table 8. Week 23, wax maturity, shows increased maximum air temperatures improve yields (0.03 tones/ $^{\circ}\text{C}$), while increased minimum soil temperatures (-0.08 tones/ $^{\circ}\text{C}$) reduce them. Here, heightened air temperatures likely support maturity while elevated soil temperatures reduce moisture content and suspend growth.

Further, wheat's shooting phase displays strong sensitivity to air temperature. Weeks 11 and 14 favor warmer minimum temperatures, while yields declined during sub-zero events. This impact likely represents a photosynthetic reduction via leaf dormancy and/or mortality. Transitioning to the heading phase, week 15, sub-zero events cease to occur and warmer minimum temperatures become undesirable. Here, plant maturity favors prolonged cool spring temperatures that maintain soil moisture, increase photosynthetic activity, and encourage growth.

MARS shooting phase precipitation and soil moisture drivers display opposing impact relationships. *February mean soil moisture* delivers a positive yield contribution, suggesting similar phase-supporting conditions as SWR's *week 15 mean soil moisture*. In contrast, *maximum monthly precipitation* displays a negative feedback, albeit at a near negligible rate and contribution magnitude (-1 to -3%). The negative feedback may indicate too much precipitation and corresponding meteorological conditions (wind, cloud cover, etc) inhibiting growth and productivity.

489

3.4 Thresholds

490

491

492

493

494

495

496

High SWR and MARS driver model performance within the MARS algorithm identifies threshold(s) and characterizes interactions before, between, and after as illustrated in Figure 5. Here, five MARS drivers display thresholds: *week 11 and 14 minimum air temperatures, week 23 maximum air and minimum soil temperatures, and maximum monthly precipitation*. With a y-intercept of 1.68 tones, impact magnitudes either increase or decrease from this amount. Within the SWR driver set, only *week 15 mean soil moisture* displayed a threshold.

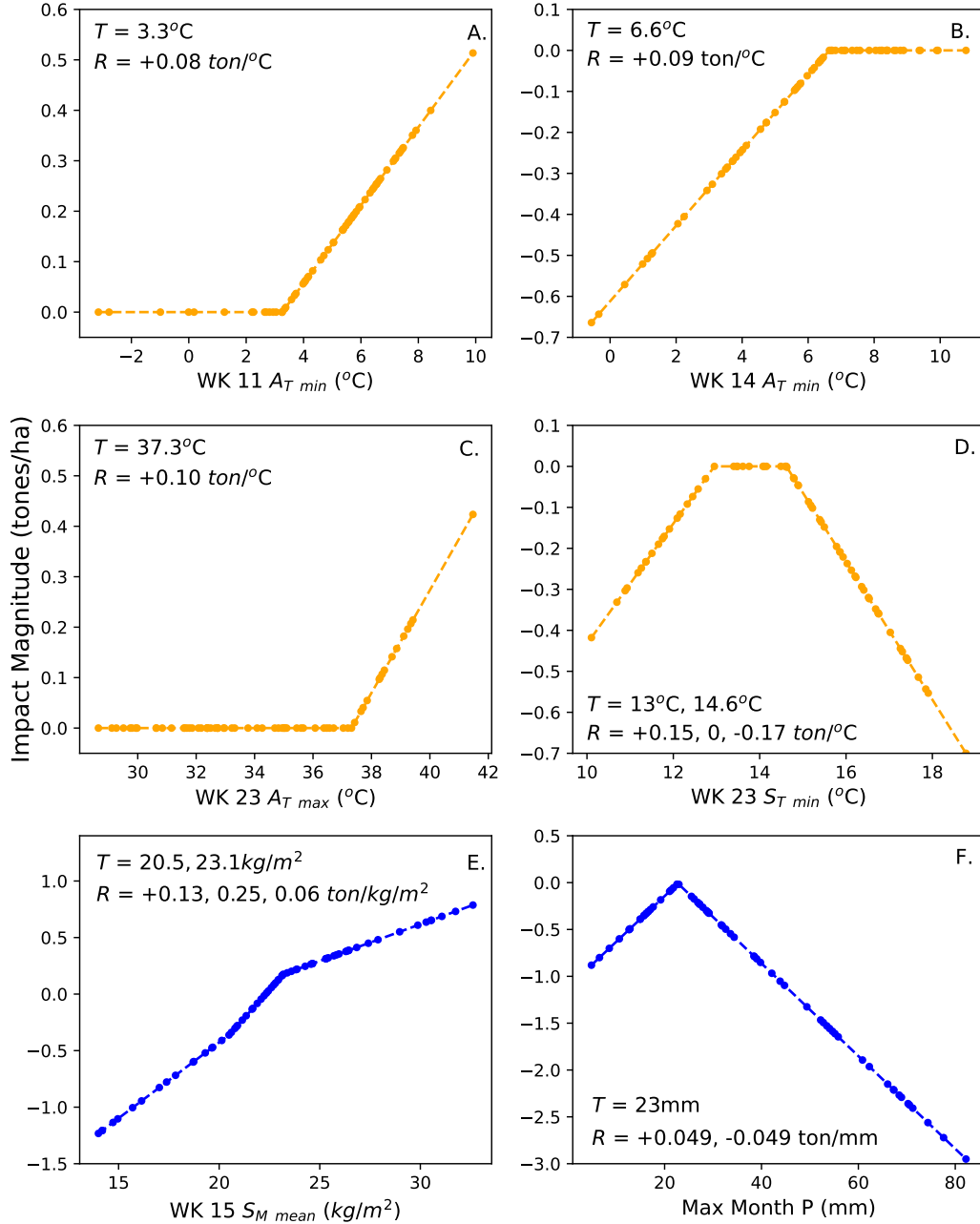


Figure 5. Optimal ranges and critical thresholds to week 11 minimum air temperature (A), week 14 minimum air temperature (B), week 23 maximum air temperature (C), week 23 minimum soil temperature (D), week 15 mean soil moisture (E), and maximum monthly precipitation (F).

All MARS air temperature drivers display positive feedbacks with temperature. Week 11 minimum and 23 maximum air temperatures show no effect until the threshold, where a strong positive impacts of $+0.08\text{tones}/^{\circ}\text{C}$ and $+0.10\text{tones}/^{\circ}\text{C}$ are respectively observed. Week 14's thresholds and rates provide key insights into shooting phase minimum air temperature. Here, air temperatures lower than 6.6°C negatively impact productivity at a rate of $-0.09\text{tones}/^{\circ}\text{C}$.

The MARS algorithm identifies optimal temperature and precipitation conditions. *Week 23 minimum soil temperature's* ideal range extends from 13°C to 14.6°C and the optimal *maximum monthly precipitation* is shown to be $23\text{mm}/\text{month}$, Figure 5(D & F). For soil temperatures, this "optimal" range demonstrates yield improvement up to 13°C ($+0.15\text{tones}/^{\circ}\text{C}$), no impact from 13°C to 14.6°C , and a strong negative impact after 14.6°C ($-0.17\text{tones}/^{\circ}\text{C}$). Monthly precipitation nearing $23\text{mm}/\text{month}$ improves yields at a rate of $+0.049\text{tones}/\text{mm}$. When monthly precipitation exceeds the threshold, an increasingly negative feedback at an equal but opposing rate is observed. This is likely a trade-off between precipitation and solar radiation favoring conditions (less cloud cover) during the shooting, heading, and flowering phases.

Week 15 mean soil moisture is the sole SWR predictor displaying two rate thresholds along a continuously positive slope. Figure 5(E) highlights thresholds at $20.5\text{kg}/\text{m}^2$ and $23.1\text{kg}/\text{m}^2$, with the transition to a positive impacts at $\sim 21.5\text{kg}/\text{m}^2$. Soil moisture levels above $\sim 21.5\text{kg}/\text{m}^2$ are important as they indicate that a positive productivity impact occurs above this threshold. When $23.1\text{kg}/\text{m}^2$ is exceeded, the slope is observed to decrease and lead to less productivity per unit increase of soil moisture.

4 Discussion

4.1 Comprehending Productivity Variances

Growing season hydro-climate conditions are not homogeneous across the Potohar plateau, with precipitation generally decreasing to the southwest and temperature increasing southward. Thus, an excellent performance measure is to use district hydro-climate statistics and characterized drivers to correctly correlate productivity differences to geography.

Jhelum's southeastern location receives the least mean and maximum precipitation, second-lowest minimum precipitation, and warmest air temperatures, yet consistently produces the highest yields. In a rainfed region, these conditions conflict with the assumption that more precipitation and cooler soil-moisture-preserving temperatures deliver optimal productivity conditions. However, the validated hydro-climate drivers and calibrated algorithms explain the greater productivity. The district's consistent precipitation, warmest minimum air temperature during tillering and shooting phases (harmful frost events are rare), and warmest mean spring temperatures ($\sim 1.5\text{-}2^{\circ}\text{C}$) support favorable photosynthetic and spike-forming conditions.

Alternatively, Chakwal displays the lowest minimum and median precipitation, greatest number of frost events, and the plateau's lowest wheat yields. Hydro-climate drivers and models help to explain this low productivity, which is a result of sub-zero events during the tillering and shooting phases. Consistent with previous research, such events seem to decrease tiller survival rate, reduce the spike number, and lower the kernel quantity per spike, compromising yield (Li et al., 2015; Zheng et al., 2018; Fuller et al., 2007). Ultimately, Chakwal's freezing temperatures and low precipitation severely inhibit its wheat productivity.

Successful algorithm/driver yield characterization across the low- and high-productivity Potohar districts provides further validation of these methods. While further research considering multiple locations and crops are necessary to endorse universal methodolog-

ical implementation, our study's success connecting hydro-climate-productivity displays strong potential for investigating climate change influences on crop productivity and improving seasonal forecasting methods.

4.2 Phenology and Predictor Significance Application

Wheat productivity displays unique phase-specific responses to growing season hydro-climate conditions. Our analysis aligns with previous wheat productivity studies in identifying tillering, shooting, and heading phases as having a strong influence on yield (Kazmi & Rasul, 2012). However, the integration of NASA earth monitoring data products and machine learning advance the research state by efficiently identifying and characterizing phase-specific hydro-climate drivers to crop productivity. As a result, this research also spotlights the shooting phase as the most hydro-climate critical phenological stage, when more than 50% of the drivers and $\sim 78\%$ of the feature importance occurs.

As expected in a rain-dependent system, precipitation and soil moisture are the most common drivers ($\sim 62\%$ total and $\sim 30\%$ each). Here, precipitation drivers occur in five of wheat's eight phenological phases, suggesting that quantity and intensity can be a limiting factor to crop productivity. Evaluating precipitation intensity-productivity interactions indicates that rates below 8mm/hr are beneficial and supportive to crop-soil water balances. This is particularly important within regions defined by steep hill slopes where runoff commonly erodes the soil and damages fields. This hypothesis is further supported by Section 3.4's precipitation and soil moisture threshold analyses. Recognizing these crop productivity responses offers a data-backed support tool directed towards policy development and infrastructure innovation. Here, features such as small dams could retain water from higher intensity rainfall for later crop irrigation, saving it from being lost to overland flow and degrading downstream water quality (Ashraf et al., 2007; Ejaz et al., 2016; Muhammad et al., 2017; Panhwar et al., 2020).

Unexpectedly, no drought-tailored metrics proved statistically significant or strong predictors to Potohar wheat productivity. This may appear counter-intuitive and a departure from previous research, which has noted that drought during specific life cycle phases can significantly decrease yields or even result in complete crop failure (Rockström & Falkenmark, 2000). While our assessment does not explicitly state that such impacts could not occur, we argue that the additional hydrologic soil-balance complexities (air temperature, soil temperature, soil moisture) and phenology-aligned approach constitute stronger influences on crop productivity than periods of drought. With respect to Potohar wheat productivity, this argument is supported by previous research investigating how the complex interactions among soil properties, temperature, incoming radiation, and other hydrological cycle components function to moderate the plant water balance. (Delworth & Manaba, 1993; Vinnikov et al., 1996; Entin et al., 2000; Wang et al., 2013). Lastly, it is also likely that the training data does not account for a prolonged drought event with a magnitude that could detrimentally impact wheat yield. Regardless, it is apparent that soil moisture characterization merits further research into crop water requirements in rainfed agrarian zones.

Phenology and hydro-climate are not limited to hydrological drivers, as temperature exhibits strong influences during the shooting and maturity phases. Minimum air temperatures, including frost and freezing events, show particularly strong negative influences on yield. By quantifying minimum air temperature's shooting phase importance, resource allocation supporting infrastructure, such as wind machines, could be installed to prevent harmful frosts from negatively impacting wheat yields. Conversely, in the transition to the heading phase, low, non-freezing temperatures are favored. Kazmi and Rasul (2009)'s findings complement our results where cooler air temperatures may preserve soil moisture levels, improving current and subsequent growing season conditions. Likewise, sustainable crop management, tilling, and residue techniques can be adopted to in-

597 sulate soils, prevent harmful low and high temperatures, and preserve soil moisture (Shen
598 et al., 2018; Sarkar et al., 2020).

599 4.3 Data/Algorithm Benefits and Limitations

600 Acquiring adequate meteorological and environmental data is a significant challenge
601 in Pakistan and many other developing nations. NASA TRMM, GPM, and GLDAS data
602 delivered continuous earth observations from 2000, featuring higher spatiotemporal res-
603 olution than what was available in-situ ($0.25^\circ \times 0.25^\circ$ vs $1.6^\circ \times 1.6^\circ$ and 3-hr vs 8-hr).
604 However, this data now exceeds the district spatial resolution crop yield (District, $\sim 1^\circ$
605 $\times 1^\circ$). It is presumed that increased model performance from sub-district spatial reso-
606 lution agricultural data could refine hydro-climate insights. Parcel-level data acquisition
607 could be up-scaled into higher-resolution district models and/or refine the regional-scale
608 Potohar model.

609 No management, soil type, or parcel-level criterion were integrated into variable
610 selection or model development due to the lack of availability. The inclusion of soil prop-
611 erties and management could increase model predictive performance as these components
612 are known to be significant productivity drivers (Lobell et al., 2002; You et al., 2009; Van It-
613 tersum et al., 2013; van Bussel et al., 2015; Gobbett et al., 2017). With their inclusion,
614 further studies could offer farmers and regional governments a framework to evaluate dif-
615 ferent crop management strategies' influence on productivity.

616 As a result of the framework's multi-model approach, algorithm benefits and lim-
617 itations emerged. MLR's functionality offers a proven foundation to evaluate scenarios
618 whose inputs are outside the range of training values, known to constrain more advanced
619 non-linear algorithms (Bekhor & Livneh, 2012; Tang et al., 2018; Everingham et al., 2016;
620 Gregorutti et al., 2017; Rodriguez-Galiano et al., 2012; Vincenzi et al., 2011). This es-
621 tablishes a platform to assess emissions-based general circulation model climate simu-
622 lations. However, this linearity also presents a limitation, as predictor-response variable
623 relationships are seldom perpetually linear. Random Forest's feature importance is a promi-
624 nent algorithm element to this study, providing a valuable tool to identify which drivers
625 and phenology phases are most important to crop yield. This algorithm, however, was
626 tedious to operate and has the potential to be computationally intensive. Lastly, the MARS
627 algorithm supplied an immense quantity of detailed insight into the piece-wise predictor-
628 productivity interactions via thresholds, rates, impact magnitudes, and optimal condi-
629 tions. While MARS provided a unique view into hydro-climate-productivity interactions,
630 the hinge functions failed to display consistent predictive performance among driver sets,
631 specifically with Random Forest drivers.

632 While each algorithm is individually qualified to perform these variable selection
633 and modeling tasks, the multi-model approach administered an effective platform to ex-
634 amine many intricacies surrounding hydro-climate impacts and agricultural productiv-
635 ity. Collectively interpreting the predictors, evaluating their respective linkages to yield,
636 and cumulative modeling results (feature importances, thresholds, and individual and
637 combined impact magnitudes) cultivates a spectrum of interaction-based process recog-
638 nition and awareness which a single model does not. Thus, we encourage future stud-
639 ies to consider multi-model approaches in their analyses.

640 5 Conclusion

641 Characterizing influential hydro-climate variables to crop productivity is critical
642 in all agriculture sectors, but especially important in rainfed regions where data avail-
643 ability is sparse, subsistence farming directly supports food security, and severe climate
644 change impacts are anticipated. We develop a framework integrating NASA TRMM, GPM,

and GLDAS data products and machine learning to identify key crop phenology-aligned hydro-climate drivers, and characterize their respective influences to productivity. This framework is demonstrated using Pakistan's Potohar plateau as a pilot study. Here, the NASA data products undergo extensive feature engineering to decompose *rabi* wheat growing season hydro-climate conditions. These components are input into three variable selection methods and modeling approaches to identify key phase-specific drivers, phenological importance, and their respective impact and thresholds to yield. As a result, we identify *rabi* wheat's shooting phase as most hydro-climate critical, being particularly responsive to sub-zero events, precipitation intensity, and total monthly precipitation. These methods are further validated by successfully capturing intra-plateau yield heterogeneity from a variety of geographically correlated hydro-climate conditions.

This broad and adaptive approach could be used on different regions and/or crop types. Our encouraging results indicate that these methods can assist future studies looking to improve forecasts and/or investigate climate change impacts on crop productivity. This establishes a platform that can improve crop yield forecasting, inform infrastructure needs, and support policy development that could help mitigate climate change impacts and facilitate food security.

Acknowledgments

This study is made possible by the support of the United States Agency for International Development (USAID) and the NASA Precipitation Measurement Mission program, Grant Numbers NNX16AD87G and NNX16AD76G. The authors also wish to thank Zak Breckenridge for technical writing support and final editing of the manuscript.

Repository and Data Availability

The datasets for this research are available in these in-text citation references: (Statistics, 2018), (Adler et al., 2003), (Rodell et al., 2004), and (Huffman et al., 2014). These datasets and reproducible models can be found at <http://doi.org/10.5281/zenodo.4509605>. Link: <https://zenodo.org/record/4509605#.YB2yw-hKiUk>. Please cite this repository as: Johnson, Ryan. (2021). whitelighting450/NASA_WEF_Wheat: NASA_WEF_ML_Wheat_Forecasting_v1 (Version v1.0). Zenodo.

References

- Adler, R. F., Huffman, G. J., Chang, A., Ferraro, R., Xie, P.-P., Janowiak, J., . . . others (2003). The version-2 global precipitation climatology project (gpcp) monthly precipitation analysis (1979–present). *Journal of hydrometeorology*, 4(6), 1147–1167.
- Adnan, S., Mahmood, R., & Khan, A. H. (2009). Water balance conditions in rain-fed areas of potohar and balochistan plateau during 1931-08. *World Applied Sciences Journal*, 7(2), 162–169.
- Agovino, M., Casaccia, M., Ciommi, M., Ferrara, M., & Marchesano, K. (2018, 05). Agriculture, climate change and sustainability: The case of eu-28. *Ecological Indicators*, 105. doi: 10.1016/j.ecolind.2018.04.064
- Ahamed, A. M. S., Mahmood, N. T., Hossain, N., Kabir, M. T., Das, K., Rahman, F., & Rahman, R. M. (2015). Applying data mining techniques to predict annual yield of major crops and recommend planting different crops in different districts in bangladesh. In *2015 ieee/acis 16th international conference on software engineering, artificial intelligence, networking and parallel/distributed computing (snpd)* (pp. 1–6).
- Alexander, L. V. (2016). Global observed long-term changes in temperature and precipitation extremes: A review of progress and limitations in ipcc assess-

- ments and beyond. *Weather and Climate Extremes*, 11, 4 - 16. Retrieved from <http://www.sciencedirect.com/science/article/pii/S2212094715300414> (Observed and Projected (Longer-term) Changes in Weather and Climate Extremes) doi: <https://doi.org/10.1016/j.wace.2015.10.007>
- Ashraf, M., Kahlowan, M. A., & Ashfaq, A. (2007). Impact of small dams on agriculture and groundwater development: A case study from pakistan. *Agricultural Water Management*, 92(1-2), 90–98.
- Awange, J., Gebremichael, M., Forootan, E., Wakbulcho, G., Anyah, R., Ferreira, V., & Alemayehu, T. (2014). Characterization of ethiopian mega hydrogeological regimes using grace, trmm and gldas datasets. *Advances in water resources*, 74, 64–78.
- Baig, M., Shahid, S., & Straquadine, G. (2013, 12). Making rainfed agriculture sustainable through environmental friendly technologies in pakistan: A review. *International Soil and Water Conservation Research*, 1, 17. doi: 10.1016/S2095-6339(15)30038-1
- Bekhor, S., & Livneh, M. (2012). Limitation of the artificial neural networks methodology for predicting the vertical swelling percentage of expansive clays. *Journal of Materials in Civil Engineering*, 25(11), 1731–1741.
- Biau, G., & Scornet, E. (2016). A random forest guided tour. *Test*, 25(2), 197–227.
- Boschetti, A., & Massaron, L. (2018). *Python data science essentials: A practitioner's guide covering essential data science principles, tools, and techniques*. Packt Publishing Ltd.
- Breiman, L. (2001). Random forests. *Machine learning*, 45(1), 5–32.
- Buitinck, L., Louppe, G., Blondel, M., Pedregosa, F., Mueller, A., Grisel, O., . . . others (2013). Api design for machine learning software: experiences from the scikit-learn project. *arXiv preprint arXiv:1309.0238*.
- Collischonn, B., Collischonn, W., & Tucci, C. E. M. (2008). Daily hydrological modeling in the amazon basin using trmm rainfall estimates. *Journal of Hydrology*, 360(1-4), 207–216.
- Cunha, R. L., Silva, B., & Netto, M. A. (2018). A scalable machine learning system for pre-season agriculture yield forecast. In *2018 ieee 14th international conference on e-science (e-science)* (pp. 423–430).
- Delworth, T., & Manaba, S. (1993). Climate variability and land-surface processes. *Advances in Water Resources*, 16(1), 3–20.
- Draper, N. R. (1981). *Smith. h. applied regression analysis*. NY: John Wiley and Sons Inc.
- Ejaz, N., Naeem, U. A., Shahmim, M. A., Elahi, A., & Khan, N. (2016). Environmental impacts of small dams on agriculture and ground water development: A case study of khanpur dam, pakistan. *Pakistan Journal of Engineering and Applied Sciences*.
- Entin, J. K., Robock, A., Vinnikov, K. Y., Hollinger, S. E., Liu, S., & Namkhai, A. (2000). Temporal and spatial scales of observed soil moisture variations in the extratropics. *Journal of Geophysical Research: Atmospheres*, 105(D9), 11865–11877.
- Everingham, Y., Sexton, J., Skocaj, D., & Inman-Bamber, G. (2016). Accurate prediction of sugarcane yield using a random forest algorithm. *Agronomy for sustainable development*, 36(2), 27.
- Friedman, J. H. (1991). Multivariate adaptive regression splines. *The annals of statistics*, 19(1), 1–67.
- Fuller, M. P., Fuller, A. M., Kaniouras, S., Christophers, J., & Fredericks, T. (2007). The freezing characteristics of wheat at ear emergence. *European Journal of Agronomy*, 26(4), 435–441.
- Geurts, P., Ernst, D., & Wehenkel, L. (2006). Extremely randomized trees. *Machine learning*, 63(1), 3–42.
- Ghani, M., Arshad, M., Shabbir, A., Shakoor, A., Mehmood, N., & Ahmad, I. (2013,

- 12). Investigation of potential water harvesting sites at potohar using modeling approach. *Pakistan Journal of Agricultural Sciences*, 50, 723-729.
- Gobbett, D., Hochman, Z., Horan, H., Garcia, J. N., Grassini, P., & Cassman, K. (2017). Yield gap analysis of rainfed wheat demonstrates local to global relevance. *The Journal of Agricultural Science*, 155(2), 282-299.
- Gregorutti, B., Michel, B., & Saint-Pierre, P. (2017). Correlation and variable importance in random forests. *Statistics and Computing*, 27(3), 659-678.
- Hertel, T., & Rosch, S. (2010, 01). Climate change, agriculture and poverty. *International Agricultural Trade Research Consortium, Proceedings Issues, 2010: Climate Change in World Agriculture: Mitigation, Adaptation, Trade and Food Security, June 2010, Stuttgart-Hohenheim, Germany*, 32.
- Hocking, R. R. (1976). A biometrics invited paper. the analysis and selection of variables in linear regression. *Biometrics*, 32(1), 1-49.
- Huffman, G., Bolvin, D., Braithwaite, Hsu, K., Joyce, R., & Xie, P. (2014). Integrated multi-satellite retrievals for gpm (imerg) [Computer software manual]. Greenbelt, MD.
- Hussain, S. S., & Mudasser, M. (2007). Prospects for wheat production under changing climate in mountain areas of pakistan—an econometric analysis. *Agricultural Systems*, 94(2), 494-501.
- IPCC. (2006). *Climate change 2006: synthesis report*. Intergovernmental Panel on Climate Change (IPCC), Geneva, Switzerland.
- IPCC. (2014). *Climate change 2014: Synthesis report. contribution of working groups i, ii and iii to the fifth assessment report of the intergovernmental panel on climate change* (Tech. Rep.). Geneva, Switzerland: Intergovernmental Panel on Climate Change.
- Jeong, J. H., Resop, J. P., Mueller, N. D., Fleisher, D. H., Yun, K., Butler, E. E., ... others (2016). Random forests for global and regional crop yield predictions. *PLoS One*, 11(6), e0156571.
- Jones, J. W., Antle, J. M., Basso, B., Boote, K. J., Conant, R. T., Foster, I., ... Wheeler, T. R. (2017). Toward a new generation of agricultural system data, models, and knowledge products: State of agricultural systems science. *Agricultural Systems*, 155, 269 - 288. Retrieved from <http://www.sciencedirect.com/science/article/pii/S0308521X1630590X> doi: <https://doi.org/10.1016/j.agry.2016.09.021>
- Karimi, V., Karami, E., & Keshavarz, M. (2018, 01). Climate change and agriculture: Impacts and adaptive responses in iran. *Journal of Integrative Agriculture*, 17, 1-15. doi: 10.1016/S2095-3119(17)61794-5
- Kazmi, D. H., & Rasul, G. (2009). Early yield assessment of wheat on meteorological basis for potohar region. *Pakistan Journal of Meteorology*, 6(11), 73-87.
- Kazmi, D. H., & Rasul, G. (2012). Agrometeorological wheat yield prediction in rainfed potohar region of pakistan. *Agricultural Sciences*, 3(02), 170.
- Kijne, J. W., Barker, R., & Molden, D. J. (2003). *Water productivity in agriculture: limits and opportunities for improvement* (Vol. 1). Cabi.
- Kim, N., Ha, K.-J., Park, N.-W., Cho, J., Hong, S., & Lee, Y.-W. (2019). A comparison between major artificial intelligence models for crop yield prediction: Case study of the midwestern united states, 2006-2015. *ISPRS International Journal of Geo-Information*, 8(5), 240.
- King, A., Markus, G., Fischer, E., Ed, H., Alexander, L., Karoly, D., ... Sarah, E. (2015, 09). The timing of anthropogenic emergence in simulated climate extremes. *Environmental Research Letters*, 10, 094015. doi: 10.1088/1748-9326/10/9/094015
- Li, X., Cai, J., Liu, F., Dai, T., Cao, W., & Jiang, D. (2015). Spring freeze effect on wheat yield is modulated by winter temperature fluctuations: Evidence from meta-analysis and simulating experiment. *Journal of agronomy and crop science*, 201(4), 288-300.

- Liakos, K., Busato, P., Moshou, D., Pearson, S., & Bochtis, D. (2018). Machine learning in agriculture: A review. *Sensors*, 18(8), 2674.
- Lobell, D. B. (2013). The use of satellite data for crop yield gap analysis. *Field Crops Research*, 143, 56–64.
- Lobell, D. B., Ortiz-Monasterio, J. I., Addams, C. L., & Asner, G. P. (2002). Soil, climate, and management impacts on regional wheat productivity in Mexico from remote sensing. *Agricultural and Forest Meteorology*, 114(1-2), 31–43.
- Mason, S., Kruczkiewicz, A., Ceccato, P., & Crawford, A. (2015). Accessing and using climate data and information in fragile, data-poor states. *International Institute for Sustainable Development: Winnipeg, MB, Canada*.
- Mathew, S., Zeng, B., Zander, K., & Singh, R. (2018, 09). Exploring agricultural development and climate adaptation in northern Australia under climatic risks. *The Rangeland Journal*, 40. doi: 10.1071/RJ18011
- Meijl, H., Havlík, P., Lotze-Campen, H., Stehfest, E., Witzke, P., Domínguez, I., ... van Zeist, W.-J. (2018, 06). Comparing impacts of climate change and mitigation on global agriculture by 2050. *Environmental Research Letters*, 13, 064021. doi: 10.1088/1748-9326/aabdc4
- Meng, T., Carew, R., Florkowski, W. J., & Klepacka, A. M. (2017). Analyzing temperature and precipitation influences on yield distributions of canola and spring wheat in Saskatchewan. *Journal of Applied Meteorology and Climatology*, 56(4), 897–913.
- Milly, P., Julio, B., Falkenmark, M., Robert, M., Zbigniew, W., Dennis, P., & Ronald, J. (2008, 01). Stationarity is dead. *Ground Water News and Views*, 4, 6-8.
- Mora, C., Spirandelli, D., Franklin, E., Lynham, J., Kantar, M., Miles, W., ... Hunter, C. (2018, 11). Broad threat to humanity from cumulative climate hazards intensified by greenhouse gas emissions. *Nature Climate Change*, 8. doi: 10.1038/s41558-018-0315-6
- Muhammad, J., Khan, A., Alam, S., & Akhtar, S. (2017). Impacts of Palai Dam on land use and cropping pattern of Mouza Qilla, District Charsadda, Khyber Pakhtunkhwa, Pakistan. *Sarhad Journal of Agriculture*, 33(1), 80–89.
- Naheed, G., & Mahmood, A. (2009). Water requirement of wheat crop in Pakistan. *Pakistan Journal of Meteorology*, 6(11), 89–97.
- NOAA. (2020). *Forecast terms*. https://www.weather.gov/bgm/forecast_terms. (Accessed: 2020-01-14)
- Panhwar, V., Zaidi, A., Ullah, A., & Edgar, T. (2020, 03). Impact of water sector interventions on economy, equity, and environment in the rainfed region of Punjab, Pakistan. *Environment, Development and Sustainability*. doi: 10.1007/s10668-020-00669-2
- Parry, M. (2019). *Climate change and world agriculture*. Taylor & Francis. Retrieved from <https://books.google.com/books?id=9uG5DwAAQBAJ>
- Pedregosa, F., Varoquaux, G., Gramfort, A., Michel, V., Thirion, B., Grisel, O., ... others (2011). Scikit-learn: Machine learning in Python. *Journal of Machine Learning Research*, 12(Oct), 2825–2830.
- Prasad, A. M., Iverson, L. R., & Liaw, A. (2006). Newer classification and regression tree techniques: bagging and random forests for ecological prediction. *Ecosystems*, 9(2), 181–199.
- Rockström, J., & Falkenmark, M. (2000). Semiarid crop production from a hydrological perspective: gap between potential and actual yields. *Critical Reviews in Plant Sciences*, 19(4), 319–346.
- Rodell, M., Houser, P., Jambor, U., Gottschalck, J., Mitchell, K., Meng, C.-J., ... others (2004). The global land data assimilation system. *Bulletin of the American Meteorological Society*, 85(3), 381–394.
- Rodriguez-Galiano, V. F., Ghimire, B., Rogan, J., Chica-Olmo, M., & Rigol-Sanchez, J. P. (2012). An assessment of the effectiveness of a random forest

- classifier for land-cover classification. *ISPRS Journal of Photogrammetry and Remote Sensing*, 67, 93–104.
- Sarkar, S., Skalicky, M., Hossain, A., Brestic, M., Saha, S., Garai, S., ... Brahmachari, K. (2020). Management of crop residues for improving input use efficiency and agricultural sustainability. *Sustainability*, 2098(12), 2–24.
- Sharma, B. R., Rao, K., Vittal, K., Ramakrishna, Y., & Amarasinghe, U. (2010). Estimating the potential of rainfed agriculture in india: Prospects for water productivity improvements. *Agricultural Water Management*, 97(1), 23–30.
- Sheffield, J., Goteti, G., & Wood, E. (2006, 07). Development of a 50-year high-resolution global dataset of meteorological forcings for land surface modeling. *Journal of Climate*, 19, 3088–3111. doi: 10.1175/JCLI3790.1
- Shen, Y., McLaughlin, N., Zhang, X., Xu, M., & Liang, A. (2018, 3). Effect of tillage and crop residue on soil temperature following planting for a black soil in northeast china. *Scientific reports*, 8(1), 4500. Retrieved from <https://europepmc.org/articles/PMC5852035> doi: 10.1038/s41598-018-22822-8
- Statistics, P. D. (2018). *Punjab development statistics 2018* (Tech. Rep.). Punjab, Pakistan: Bureau of Statistics, Planning and Development Department.
- Sun, H., Shen, Y., Yu, Q., Flerchinger, G. N., Zhang, Y., Liu, C., & Zhang, X. (2010). Effect of precipitation change on water balance and wue of the winter wheat–summer maize rotation in the north china plain. *Agricultural Water Management*, 97(8), 1139–1145.
- Tang, C., Garreau, D., & von Luxburg, U. (2018). When do random forests fail? In *Advances in neural information processing systems* (pp. 2983–2993).
- UCR. (2018). *Multivariate adaptive regression splines*. University of California, Riverside. Retrieved from <http://uc-r.github.io/2018/09/08/mars/>
- Ullah, W., Wang, G., Ali, G., Tawia Hagan, D. F., Bhatti, A. S., & Lou, D. (2019). Comparing multiple precipitation products against in-situ observations over different climate regions of pakistan. *Remote Sensing*, 11(6), 628.
- van Bussel, L. G., Grassini, P., Van Wart, J., Wolf, J., Claessens, L., Yang, H., ... others (2015). From field to atlas: Upscaling of location-specific yield gap estimates. *Field Crops Research*, 177, 98–108.
- Van Ittersum, M. K., Cassman, K. G., Grassini, P., Wolf, J., Titttonell, P., & Hochman, Z. (2013). Yield gap analysis with local to global relevance—a review. *Field Crops Research*, 143, 4–17.
- Vincenzi, S., Zucchetta, M., Franzoi, P., Pellizzato, M., Pranovi, F., De Leo, G. A., & Torricelli, P. (2011). Application of a random forest algorithm to predict spatial distribution of the potential yield of ruditas philippinarum in the venice lagoon, italy. *Ecological Modelling*, 222(8), 1471–1478.
- Vinnikov, K. Y., Robock, A., Speranskaya, N. A., & Schlosser, C. A. (1996). Scales of temporal and spatial variability of midlatitude soil moisture. *Journal of Geophysical Research: Atmospheres*, 101(D3), 7163–7174.
- Wang, S., Fu, B., Gao, G., Liu, Y., & Zhou, J. (2013). Responses of soil moisture in different land cover types to rainfall events in a re-vegetation catchment area of the loess plateau, china. *Catena*, 101, 122–128.
- Worqlul, A., Maathuis, B., Adem, A., Demissie, S., Langan, S., & Steenhuis, T. (2014, 07). Comparison of trmm, mpeg and cfsr rainfall estimation with the ground observed data for the lake tana basin, ethiopia. *Hydrology and Earth System Sciences Discussions*, 11, 8013–8038. doi: 10.5194/hessd-11-8013-2014
- You, L., Rosegrant, M. W., Wood, S., & Sun, D. (2009). Impact of growing season temperature on wheat productivity in china. *Agricultural and Forest Meteorology*, 149(6–7), 1009–1014.
- Zheng, D., Yang, X., Mínguez, M. I., Mu, C., He, Q., & Wu, X. (2018). Effect of freezing temperature and duration on winter survival and grain yield of winter wheat. *Agricultural and forest meteorology*, 260, 1–8.